Theoretical Study of Model Compound I Complexes of Horseradish Peroxidase and Catalase

Ping Du and Gilda H. Loew
Molecular Research Institute, Palo Alto, California 94304 USA

ABSTRACT Theoretical studies of the electronic structure and spectra of models for the ferric resting state and Compound I intermediates of horseradish peroxidase (HRP-I) and catalase (CAT-I) have been performed using the INDO-RHF/CI method. The goals of these studies were twofold: i) to determine whether the axial ligand of HRP is best described as imidazole or imidazolate, and ii) to address the long-standing question of whether HRP-I and CAT-I are a_{1u} and a_{2u} π cation radicals. Only the imidazolate HRP-I model led to a calculated electronic spectra consistent with the experimentally observed significant reduction in the intensity of the Soret band compared with the ferric resting state. These results provide compelling evidence for significant proton transfer to the conserved Asp residue by the proximal histidine. The origin of the observed reduction of the Soret band intensity in HRP-I and CAT-I spectra has been examined and found to be caused by the mixing of charge transfer transitions into the predominantly porphyrin π-π transitions. For both HRP-I and CAT-I, the a_{1u} porphyrin π cation state is the lowest energy, and it is further stabilized by both the anionic form of the ligand and the porphyrin ring substituents of protoporphyrin-IX. The calculated values of quadrupole-splitting observed in the Mossbauer resonance of HRP-I and CAT-I are similar for the a_{1u} and a_{2u} π cation radicals. Electronic spectrum of the a_{1u} π cation radical of HRP-I are more similar to the observed spectra, whereas the spectra of both a_{1u} π and a_{2u} π cation radicals of CAT-I resemble the observed spectra. These results also indicate the limitations of using any one observable property to try to distinguish between these states. Taken together, comparison of calculated and observed properties indicate that there is no compelling reason to invoke the higher energy a_{2u} π cation radical as the favored state in HRP-I and CAT-I. Both ground-state properties and electronic spectra are consistent with the a_{1u} π cation radical.

INTRODUCTION

Compound I is a key intermediate in the biological actions of horseradish peroxidase (HRP), catalase (CAT), and other metabolizing heme proteins (Dunford, 1991; Bosshard et al., 1991; Hewson and Hager, 1978). Although the enzymatic cycles of both HRP and CAT require stoichiometric concentration of hydrogen peroxide, H_2O_2, the biological functions of these two enzymes are very different. HRP utilizes H_2O_2 to catalyze the oxidation of aromatic amines and phenols, whereas CAT catalyzes the oxidation of another H_2O_2 to O_2 (Eqs. 1a–2b). As shown in Eqs. 1a and 2a, the first stable intermediate in the catalytic cycles of HRP and CAT, Compound I, is formed by the transfer of one oxygen atom from H_2O_2 to the ferric iron of the heme in the resting states of these two enzymes. Compound I of HRP (HRP-I) performs a one-electron oxidation of a substrate forming another stable intermediate, Compound II (HRP-II, Eq. 1b), which performs a second subsequent one-electron oxidation of another substrate and returns to the resting state (Eq. 1c). By contrast, Compound I of CAT (CAT-I) performs a concerted two-electron oxidation of another molecule of H_2O_2 and returns directly to the resting state. (Eq. 2b) The ability of catalase to convert two H_2O_2 to H_2O and O_2 gives it the unique function of eliminating hydrogen peroxide, a hazardous, partially reduced product of molecular oxygen in the respiration system of mammals.

$$HRP + H_2O_2 \rightarrow HRP\text{-}I + H_2O \quad (1a)$$

$$HRP\text{-}I + AH \rightarrow HRP\text{-}II + A^{+\bullet} \quad (1b)$$

$$HRP\text{-}II + AH + H^+ \rightarrow HRP + A^{+\bullet} + H_2O \quad (1c)$$

$$CAT + H_2O_2 \rightarrow CAT\text{-}I + H_2O \quad (2a)$$

$$CAT\text{-}I + H_2O_2 \rightarrow CAT + H_2O + O_2 \quad (2b)$$

The distinct difference of the functions of HRP and CAT raises the possibility that it is related to the possible differences in the electronic structures of HRP-I and CAT-I, the bioactive form of each enzyme. The catalytic centers of both enzymes have a protoporphyrin-IX prosthetic group but differ in the axial ligand, with a histidine residue as the proximal ligand in HRP and a tyrosine residue as the proximal ligand in CAT. A variety of spectroscopic methods indicate that both HRP-I and CAT-I are iron-oxo (Fe=O) porphyrin radical cation complexes. Mossbauer spectra of HRP-I are consistent with an Fe(IV) oxidation state for the heme iron (Moss et al., 1969; Schulz et al., 1979, 1984), and the porphyrin radical cation was first proposed (Dolphin et al., 1971) and then observed by ESR spectroscopy (Schulz et al., 1979). Oxygen atom ligation of Fe(IV) in Compound I was detected in ^{18}O-labeled chloroperoxidase (Hager et al., 1972), another heme protein, and by EXAFS studies (Penner-Hahn et al., 1986).

Although evidence from a variety of experimental and theoretical studies clearly indicate the nature of the Fe(IV S

Received for publication 5 July 1994 and in final form 12 October 1994.
Address reprint requests to Dr. Gilda Loew, Molecular Research Institute, 845 Page Mill Rd., Palo Alto, CA 94304. Tel.: 415-424-9985; 415-424-9501; E-mail: loew@montara.molres.org.

0006-3495/95/01/69/12 $2.00

= 1)=O moiety in the Compound I intermediate of peroxidase, the question of whether the third unpaired spin is predominantly distributed in a porphyrin π a_{1u} or a_{2u} orbital is still unresolved despite much effort. Over the years, a variety of properties including optical absorption spectra, hyperfine splittings in NMR spectra, resonance Raman spectra, and quadrupole splitting in Mossbauer resonance spectra have been examined and used to try to identify the preferred cation radical for HRP-I and CAT-I. Based on optical spectra comparisons, it was long thought that HRP-I was a $^2A_{2u}$ π cation radical (Dolphin et al., 1971; Dolphin, 1981) and CAT-I a $^2A_{1u}$ π cation radical. This assumption was based on subtle differences in their visible spectra in which the Q band of HRP-I has a peak at 17 kK and a shoulder near 15 kK whereas CAT-I has a peak at 15 kK with shoulders near 16 and 18 kK. It was also thought that the spectra of HRP-I resembled that of an octaethylporphyrin(OEP) complex Co III (OEP) $(ClO_4)_2$, assumed to be a $^2A_{2u}$ ground state, whereas the spectra of CAT-I resembled that of Co(III) (OEP) $(Br)_2$ thought to have a $^2A_{1u}$ ground state. However, the ground states of the model compounds have been questioned, and both are now thought to be predominantly $^2A_{1u}$ in character (Chance et al., 1984). Also, more detailed spectroscopic studies of both model porphyrin π cation radicals and the Compound I intermediate of intact proteins have shown that absorption spectra are not reliable indicators of their ground states (Chance et al., 1984; Ridley and Zerner, 1973, 1976; Bacon, 1976; Bacon and Zerner, 1979; Edwards et al., 1987, 1986, 1988; Pauncz, 1979; Du et al., 1991; Piciulo et al., 1974). In fact, the visible spectra of beef liver catalase-I is more similar to HRP-I (Browett and Stillman, 1981), arguing against using similarities and differences in optical spectra alone to determine the most favored π cation radical in Compound I intermediates.

In principle, the a_{1u} and a_{2u} π cation radicals can be distinguished by ESR and NMR spectra, because an unpaired electron in the $3a_{2u}$ orbital has significant density on the meso carbon and N_{pyr} atoms of the porphyrin, whereas the coefficients of the $1a_{1u}$ orbital on these atoms are zero. Unfortunately, the ESR signal of the porphyrin radical cation is broadened by the coupling of the unpaired electron with the ferryl iron (S = 1), resulting in a broad, featureless band (Schulz et al., 1979, 1984). Similar difficulty was encountered in the NMR experiment, in which the chemical shift caused by the radical densities on the meso and β carbons could not be observed because of protein interference (Hanson et al., 1981; La Mar et al., 1989). Additionally, nonzero spin density on N_{pyr} in the a_{1u} radical cation can result from the deviation of the heme from D_{4h} symmetry caused by the protein environment, the axial ligands, or spin polarization of the porphyrin π orbitals, as found in UHF calculations that allow such interactions (Loew and Herman, 1980). Thus, the small spin delocalization observed on N_{pyr} in the ENDOR study of HRP-I (Roberts et al., 1981), although suggestive, does not provide definitive evidence for an a_{2u} π radical cation ground state for HRP-I.

Resonance raman (*r*R) spectroscopy has also more recently been used to try to elucidate the nature of the π cation radical of HRP-I and CAT-I (Chuang and Van Wart, 1992). The inference drawn from these studies is that the a_{2u} radicals are favored. These deductions were based on small observed shifts in the C_β—C_β and C_α—C_m stretching frequencies between Compound II and Compound I and on the assumption that these shifts are caused entirely by electronic modulation of bond strengths depending on whether the a_{1u} or a_{2u} orbital is singly occupied. These deductions have three major weaknesses: i) the shifts observed are extremely small ≤ 10 cm^{-1} and difficult to reproduce; ii) the presumed origin of these shifts has not been verified by any independent means. For example, no calculations, have been made to test the key assumption that observed C_β—C_β and C_α—C_m bond weakening and bond strengthening between Compound II and Compound I is due entirely to whether the electron is removed from an a_{1u} or a_{2u} orbital; iii) the small observed shifts could be due to other factors, the most obvious being a very small change in C_β—C_β and C_α—C_m bond lengths caused by a change in the oxidation state of the porphyrin in going from Compound II to Compound I.

Evidence for the lack of correlation between a_{1u} or a_{2u} orbital occupancy and C_β—C_β and C_α—C_m stretching frequency comes directly from the *r*R results themselves. These frequencies are the same for Compound I and the ferric states of HRP and CAT, despite the fact that the a_{1u} and a_{2u} orbital occupancies are different in these two states of each enzyme. Conversely, these frequencies are different for the ferric resting state and Compound II forms of each protein in which the a_{1u} or a_{2u} orbital occupancy is the same. Thus, there is no correlation between occupancy of a_{1u} or a_{2u} orbitals and small changes in porphyrin stretching frequency.

Despite a great deal of effort, no one experimental method has been able to definitively elucidate the nature of the preferred π cation state of HRP-I or CAT-I. The techniques of computational chemistry, in conjunction with the experimental observations, can help to probe further this question by calculating the relative energies and observable properties to be expected for both the a_{1u} and a_{2u} π cation radical states of model HRP-I and CAT-I and determining which, if any, are most consistent with experiment. To this end, the spectra of a number of model complexes have been calculated to elucidate the origin of the reduction of the Soret band intensity of HRP-I and CAT-I relative to their resting states, a key characteristic of the optical spectra of both HRP-I and CAT-I. For example, for HRP-I, the extinction coefficient of the Soret decreases to 0.54×10^5 M^{-1} cm^{-1} from 1.02×10^5 M^{-1} cm^{-1} of the resting state (Dunford, 1982). For CAT-I it decreases to 1.8×10^5 M^{-1} cm^{-1} from 4.0×10^5 M^{-1} cm^{-1} of the resting state (Palcic and Dunford, 1980). Similar reductions have also been observed for yeast (Palcic et al., 1980) and animal peroxidases (Harrison et al., 1980), indicating that this approximate twofold reduction in the Soret band strength is a common property of Compound I of heme proteins. In addition, spin densities, quadrupole splitting in Mossbauer resonance spectra, and relative energies of

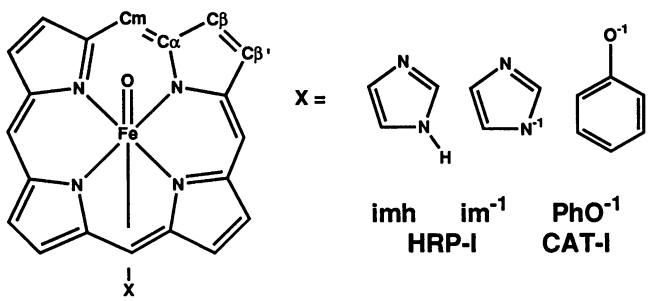

FIGURE 1 Model complexes for HRP-I and CAT-I. The porphyrin is in the *xy* plane, and the ligand X is in the *xz* plane. The overal symmetry is C_s.

different π cation states were calculated as supporting criteria for selecting the candidates among different model complexes.

Because the axial ligands are the major differences in these active site models, the nature of these ligands has also been addressed. In particular, the question of whether the HRP ligand is best described as imidazole or imidazolate was also considered.

MATERIALS AND METHODS

A spin-restricted, open-shell INDO/S method was used for all calculations reported here (Ridley and Zerner, 1973, 1976; Bacon, 1976; Bacon and Zerner, 1979; Edwards and Zerner, 1987; Edwards et al., 1986, 1988). Spectra calculations included only single excitations in the configuration interaction (CI—S). CI configurations were generated within a selected MO space using the Rumer diagram technique (Pauncz, 1979). For the ferric resting state models, a sextet reference configuration was used to calculate the spectra. For the HRP-I and CAT-I species, both the a_{1u} and a_{2u} radical cations were used as reference configurations to calculate spectra. Recent spectral calculations on model Compound II complexes of peroxidases have demonstrated the ability of this method to predict the detailed features and differences in the spectra of different models (Paeng and Kincaid, 1988). In addition, a number of other properties were calculated for each state including their relative energies, electron and spin distributions, and quadrupole splittings observed in Mossbauer resonance.

The geometry of the porphyrin was taken from the x-ray crystal structure of iron tetraphenylporphyrin (Piciulo et al., 1974) and has been regularized to D_{4h} symmetry for calculation of the spectra. The distance used between the iron atom and the pyrrole nitrogen atoms of the porphyrin is 2.01 Å, consistent with the bond length in CAT-I and HRP-I as estimated in x-ray absorption studies (Chance et al., 1984). A bond length of 1.65 Å was chosen for the iron-oxo group for both HRP-I and CAT-I, as found in the EXAFS studies of HRP-I (Anderson and Dawson, 1991). Two different ligands were used to model the resting state HRP and HRP-I, an imidazole (imh) and an imidazolate (im^{-1}) group. For all HRP and HRP-I models (HRP/imh, HRP/im^{-1}, HRP-I/imh, and HRP-I/im^{-1}), the Fe—N_ϵ bond length is 2.02 Å, as found in the crystal structure of cytochrome *c* peroxidase (CCP) (Poulos and Finzel, 1984), another peroxidase with an axial histidine ligand. The HRP and HRP-I model with an im^{-1} ligand was included because of recent evidence from NMR spectra (de Ropp et al., 1985) of proton transfer from the proximal histidine residue to a nearby aspartate. For CAT-I, a phenolate group (PhO^{-1}) was used as a model of the tyrosine ligand of iron with an Fe-OPh^{-1} bond length of 1.89 Å and the angle between the Fe-OPh^{-1} bond and the Ph plane of 143.0° as found in the crystal structure of CAT (Fita and Rossman, 1985).

The model systems used in the calculations are shown in Fig. 1, with the *z* axis normal to the heme plane. Although the geometries do not have D_{4h} symmetry, D_{4h} symmetry labels (e.g., $3a_{2u}$) have been used for the molecular orbitals of the porphyrin. For the orbitals mostly localized on the Fe=O, σ and π labels are used, such as Fe=O π. The orbitals localized on the axial ligands are labeled as follows: imhπ_3 for the third π orbital of the imidazole ring, phπ_3 for the third orbital of the benzene ring of the phenolate ligand, etc. To reduce the size of the CI matrix, C_s symmetry was imposed on the electronic wave functions.

To determine the substituent effect on the relative energies of the a_{1u} and a_{2u} radical cations ($a_{1u}^{\bullet+}$ and $a_{2u}^{\bullet+}$), an HRP-I model with the full protoporphyrin-IX with a geometry as in CCP was included in the study. The coordinates for the heavy atoms of protoporphyrin-IX were taken directly from the crystal structure (Poulos and Finzel, 1984). Hydrogen atoms were added with standard bond lengths and angles. The two carboxylate groups were replaced by CH=O groups to reduce the overall charge and help ROHF convergence. Calculations of the resting state of CCP have shown that this replacement does not affect the estimated relative energies of different spin states (Du and Loew).

RESULTS AND DISCUSSION

Relative energies and properties of Compound I

Table 1 shows the calculated relative energies of $a_{2u}^{\bullet+}$ and $a_{1u}^{\bullet+}$ π cation radicals, their spin distributions and quadrupole splittings for different models of HRP-I and for CAT-I. For all models of HRP-I, the $a_{1u}^{\bullet+}$ state is found to be the ground state. The relative energies of the $a_{2u}^{\bullet+}$ state vary from 6.9 kcal/mol in the imh model, to 7.4 kcal/mol in the im^{-1} model, to 10.4 kcal/mol of the protoporphyrin-IX model with an im^{-1} ligand. Thus, deprotonation of the imidazole and addition of protoporphyrin-IX porphyrin ring substituents increasingly favor the a_{1u} π cation radical state. As shown in Table 1, for the two HRP-I models with the im^{-1} ligand (HRP-I/im^{-1}), an additional low-lying state with the unpaired electron occupying the ligand $im^{-1}\pi_3$ orbital rather than either porphyrin π orbital was also found. This state corresponds to an electron transfer from the ligand to the porphyrin. The energy of this $im^{-1}\pi_3$ radical cation ($im^{-1}\pi_3^{\bullet+}$) was calculated to be 3.3 kcal/mol and 11.5 kcal/mol above the a_{1u} radical cation for the two models, respec-

TABLE 1 Relative energies and properties of low-lying quartet states of model HRP-I and CAT-I with ROHF calculations

	HRP-I/imh, porphine		HRP-I/im^{-1}, porphine			HRP-I/im^{-1}, protoporphyrin-IX			CAT-I	
	$a_{1u}^{\bullet+}$	$a_{2u}^{\bullet+}$	$a_{1u}^{\bullet+}$	$a_{2u}^{\bullet+}$	$im^{-1}\pi_3^{\bullet+}$	$a_{1u}^{\bullet+}$	$a_{2u}^{\bullet+}$	$im^{-1}\pi_3^{\bullet+}$	$a_{1u}^{\bullet+}$	$a_{2u}^{\bullet+}$
$E(a_{2u})-E(a_{1u})$ (kcal/mol)	0.00	6.91	0.00	7.37	3.28	0.00	10.42	11.5	0.00	4.44
Spin Population Fe $3d_{xz}$	0.68	0.68	0.70	0.70	0.70	0.73	0.74	0.73	0.71	0.70
$3d_{yz}$	0.68	0.68	0.71	0.70	0.71	0.67	0.68	0.65	0.73	0.73
Spin Population O $2p_x$	0.30	0.30	0.28	0.28	0.29	0.24	0.23	0.25	0.26	0.27
$2p_y$	0.29	0.30	0.27	0.27	0.27	0.24	0.24	0.25	0.24	0.23
ΔE_Q	1.45	1.47	1.34	1.35	1.58	1.28	1.32	1.55	1.41	1.43

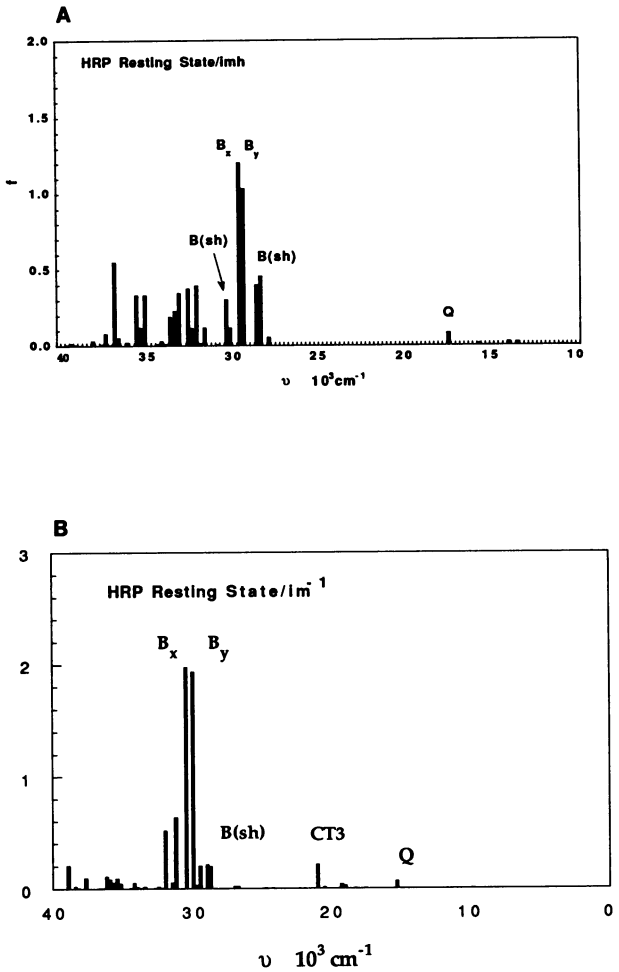

FIGURE 2 Calculated absorption spectra of HRP resting state with (*A*) an imidazole ligand, and (*B*) an imidazolate ligand.

tively. Therefore, the substituents of the protoporphyrin-IX model significantly stabilize the a_{1u} radical cation not only relative to the $a_{2u}^{\bullet+}$ but also to the $im^{-1}\pi_3^{\bullet+}$ cation, thus strengthening the prediction of the $a_{1u}^{\bullet+}$ as the ground state of HRP-I. CAT-I was also calculated to have an $a_{1u}^{\bullet+}$ as its ground state, with the $a_{2u}^{\bullet+}$ estimated to be 4.4 kcal/mol higher in energy. Thus, based on the relative ROHF energies, the $a_{1u}^{\bullet+}$ was predicted to be the ground state for both HRP-I and CAT-I.

The calculated spin densities on the Fe=O π orbitals for the a_{1u}, a_{2u}, and im^{-1} π radical cations (Table 1) are very similar for all model complexes of Compound I. Large spin densities are located on the Fe $3d_{xz}$ and $3d_{yz}$ orbitals (total 1.36–1.46), with significant amount of spin delocalized on the O $2p_x$ and $2p_y$ orbitals (total 0.47–0.60), giving it radical character. This delocalization is a direct result of the out-of-phase combination of Fe $3d_\pi$ and O $2p_\pi$ in the antibonding orbitals (Fe=O π^*) occupied by the two unpaired electrons. The spin density obtained in the oxygen is in close agreement with the 0.5 estimated from ENDOR experiment (Roberts et al., 1981) and the 0.40 of the previous theoretical calculations on model Compound II (Du et al., 1991), but significantly larger than the 0.07 of the extended Huckel calculations on model Compound I (Hanson et al., 1981). However, the similarity in spin population for all the low-lying π radical cations does not allow the use of spin populations on the ferryl oxygen moiety to distinguish the $a_{1u}^{\bullet+}$ and $a_{2u}^{\bullet+}$ radical cations of HRP-I and CAT-I from each other through ESR.

The nuclear quadrupole splittings (ΔE_Q) calculated from the SCF wave functions are similar for the a_{1u} and a_{2u} states within a given model. The ΔE_Q for the $im^{-1}\pi_3^{\bullet+}$, however, was found to be significantly larger in both the porphine and protoporphyrin-IX models of HRP-I. Experimentally observed values of ΔE_Q for HRP-I (1.20 from Moss et al., 1969 and 1.40 from Schultz et al., 1984) are in better agreement with the a_{1u} and a_{2u} states than with the $im^{-1}\pi_3$ state, providing evidence for these two states as possible candidates of the ground state of HRP-I. Because the calculated spin distributions on the oxygen and nuclear quadrupole splittings

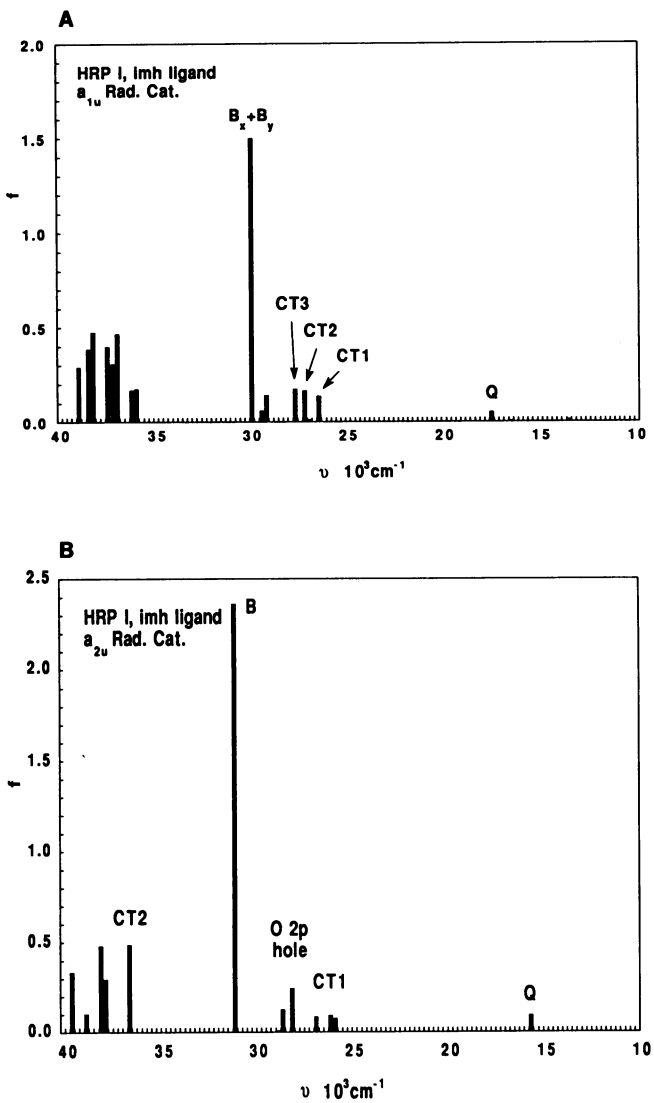

FIGURE 3 Calculated absorption spectra of HRP-I with the imh ligand (*A*) in the a_{1u} radical cation state and (*B*) in the a_{2u} radical cation state.

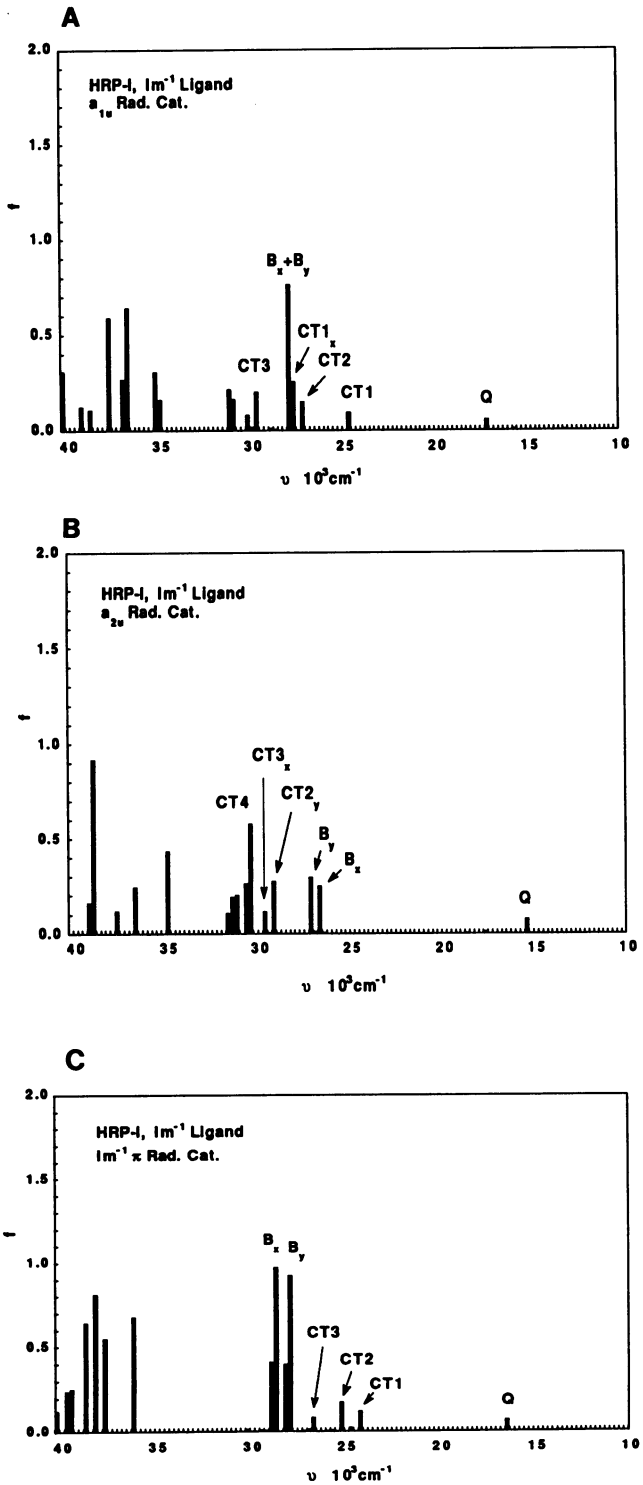

FIGURE 4 Calculated absorption spectra of HRP-I with the im^{-1} ligand (*A*) in the a_{1u} radical cation state, (*B*) in the a_{2u} radical cation state, and (*C*) in the im^{-1} π_3 radical cation state.

of $a_{1u}^{\bullet+}$ of both HRP-I and CAT-I are consistent with experiment, and because $a_{1u}^{\bullet+}$ is significantly lower in energy than $a_{2u}^{\bullet+}$, selection of the $a_{1u}^{\bullet+}$ state as the most favorable state of both enzymes is the most compatible with the experimental and theoretical results for ground-state properties.

The calculated spectra of HRP-I

To examine further the consistency with experiment of an $a_{1u}^{\bullet+}$ ground state for both HRP-I and CAT-I, the electronic absorption spectra were calculated for the following nine species: i) the resting state HRP with imh ligand (sextet) (Fig. 2 *A*); ii) the resting state HRP with im^{-1} ligand (sextet) (Fig.2 *B*); iii) the HRP-I/imh, $a_{1u}^{\bullet+}$ (Fig. 3 *A*); iv) the HRP-I/imh, $a_{2u}^{\bullet+}$ (Fig. 3 *B*); v) HRP-I/im^{-1}, $a_{1u}^{\bullet+}$ (Fig. 4 *A*); vi) the HRP-I/im^{-1}, $a_{2u}^{\bullet+}$ (Fig. 4 *B*); vii) the HRP-I/im^{-1}, $im^{-1}\pi_3^{\bullet+}$ (Fig. 4 *C*); viii) CAT-I, $a_{1u}^{\bullet+}$ (Fig. 5 *A*); and ix) the CAT-I, $a_{2u}^{\bullet+}$ (Fig. 5 *B*). The energies of the active MOs used for the Cl—S spectra calculations of compound I species are listed in Table 2. A similar set of MOs were used for the resting state models of HRP. These orbitals include the three half filled MOs, 8 to 9 unoccupied, and 14 to 15 occupied MOs. These MOs are the σ and π orbitals of the Fe=O fragment for model Compound I complexes, most of the π and π^* MOs of the porphyrin, some of the ligand π MOs, and all of the Fe 3d orbitals. Electron excitations within these MOs should account for the configurations with the most important contributions to the excited states because only low energy bonding and high energy antibonding orbitals are discarded.

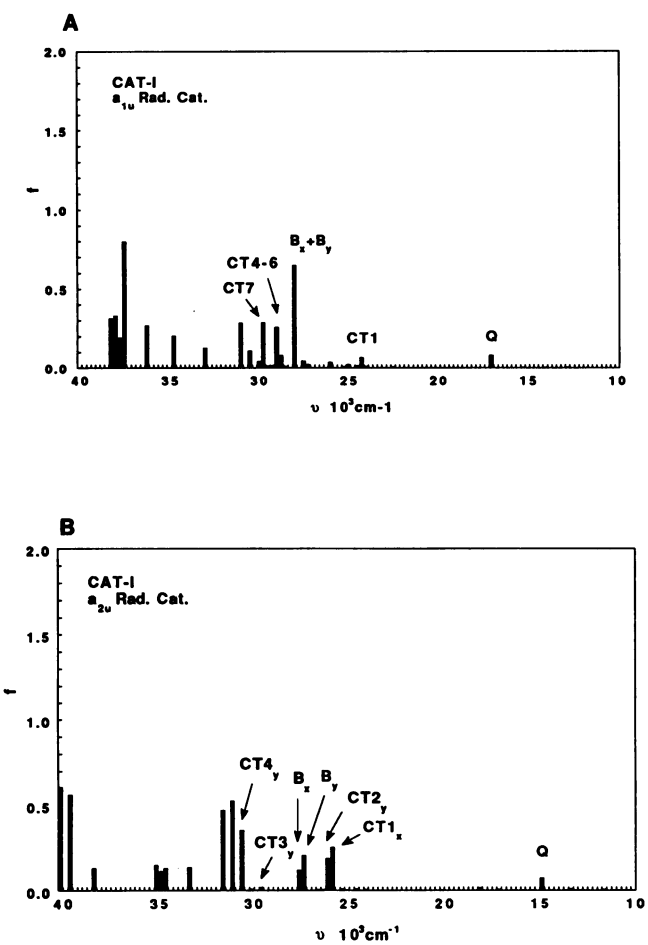

FIGURE 5 Calculated absorption spectra of CAT-I (*A*) in the a_{1u} radical cation state and (*B*) in the a_{2u} radical cation state.

TABLE 2 Energies of the active MOs in CIS calculations for spectra of model HRP-I and CAT-I (eV)

HRP-I/imh			HRP-I/im^{-1}				CAT-I		
	$a_{1u}^{\bullet+}$	$a_2^{\bullet+}$		$a_{1u}^{\bullet+}$	$a_{2u}^{\bullet+}$	$im^{-1}\pi_3^{\bullet+}$		$a_{2u}^{\bullet+}$	$a_{1u}^{\bullet+}$
Unoccupied MOs									
						im σ^* 1.91	$5e_{gy}$	1.62	1.46
imh π_5^*	−1.73	−1.63	$5e_{gx}$	1.41	1.28	$3b_{2u}$ 1.36	$5e_{gy}$	1.62	1.46
$3b_{2u}$	−1.86	−2.01	$5e_{gy}$	1.41	1.27	σ^* 1.09	phπ_4^*	1.40	1.52
σ^*	−1.99	−1.84	σ^*	0.89	1.10	$2b_{1u}$ 0.27	σ^*	1.14	1.34
imh π_4^*	−2.79	−2.68	$3b_{2u}$	0.75	0.64	d_{xy} 0.21	$3b_{2u}$	0.98	0.86
$2b_{1u}$	−2.95	−2.82	d_{xy}	−0.25	−0.05	imπ_5^* −0.09	$d_{x^2-y^2}$	0.06	0.27
d_{xy}	−3.01	−2.87	$2b_{1u}$	−0.44	−0.33	imπ_4^* −0.52	$2b_{1u}$	−0.25	−0.16
$4e_{gy}$	−4.63	−4.57	$4e_{gy}$	−2.07	−2.00	$4e_{gy}$ −1.34	$4e_{gy}$	−1.87	−1.80
$4e_{gx}$	−4.64	−4.57	$4e_{gx}$	−2.08	−2.00	$4e_{gx}$ −1.35	$4e_{gx}$	−1.87	−1.80
Occupied MOs									
$1a_{1u}$	−9.47	−9.65	$1a_{1u}-im\pi_3$	−6.88	−7.07	$3a_{2u}$ −6.67	$1a_{1u}$	−6.69	−6.87
$m3a_{2u}$	−10.15	−9.80	$3a_{2u}$	−7.53	−7.15	π^*_x −9.57	$3a_{2u}$	−7.32	−6.92
π^*_y	−12.77	−12.62	π^*_x	−10.03	−9.81	π^*_y −9.68	π^*_x	−9.54	−9.32
π^*_x	−12.79	−12.65	π^*_y	−10.07	−9.85	imπ_3 −10.22	π^*_y	−9.79	−9.53
			imπ_3+$1a_{1u}$	−6.96	−6.79	$1a_{1u}$ −6.32			
$3e_{gy}-\pi_y$	−11.70	−11.72	imπ_2	−8.49	−8.33	$3e_{gx}-\pi_x$ −8.65	phπ_3	−7.57	−7.46
$3e_{gx}-\pi_x$	−11.71	−11.73	$3e_{gx}-\pi_x$	−9.06	−9.05	$3e_{gy}-\pi_y$ −8.65	phπ_2	−8.55	−8.43
imhπ_3-2b_{2u}	−11.86	−11.81	$2a_{2u}-Nsp^2$	−9.09	−9.62	$2a_{2u}$ −8.97	$3e_{gx}-\pi_x$	−8.83	−8.81
$2a_{2u}-\sigma$	−11.88	−12.01	$3e_{gy}-\pi_y$	−9.10	−9.07	$2b_{2u}$ −9.05	$3e_{gx}-\pi_y$	−8.84	−8.82
$2b_{2u}$+imhπ_3	−12.15	−12.19	$2b_{2u}$	−9.51	−9.57	$2e_{gx}$ −9.41	$O_1p_y+O_2p_y$	−9.12	−8.86
$2e_{gx}$	−12.34	−12.33	Nsp^2+2a_{2u}	−9.67	−9.12	$2e_{gy}$ −9.43	$2a_{2u}$	−9.13	−9.24
$2e_{gy}$	−12.36	−12.35	$2e_{gy}$	−9.85	−9.83	im$\pi_2-\pi_y$ −10.19	$2b_{2u}$	−9.29	−9.35
π_y−imhπ_2	−13.46	−13.34	$2e_{gx}+Nsp^2$	−9.86	−9.83	$d_{x^2-y^2}$ −10.33	$2e_{gx}$	−9.66	−9.64
$d_{x^2-y^2}$	−13.55	−13.40	$d_{x^2-y^2}$	−10.77	−10.56	π_x −10.76	$2e_{gy}$	−9.66	−9.65
π_x	−13.93	−13.82	π_x	−11.11	−10.98	$1b_{1u}$ −11.01	$O_1p_x+O_2p_x$	−10.33	−10.17
$1b_{1u}-\sigma$	−14.06	−14.01	π_y	−11.19	−11.06	σ −11.24	$3d_{xy}$	−10.46	−10.24
σ+$1b_{1u}$	−14.35	−14.21	σ	−11.21	−11.09	π_y+imπ_2 −11.32	π_y	−11.14	−11.01
imh$\pi_2+\pi_y$	−14.66	−14.56	$1b_{1u}$	−11.50	−11.43		$\sigma-\pi_x$	−11.24	−11.08

The energies of the half-occupied orbitals, including Fe = Oπ^*_x and Fe = Oπ^*_y, and one of $3a_{2u}$, $1a_{1u}$, and $im^{-1}\pi_3$ are underlined.

Comparison of the calculated oscillator strengths of the Soret (B) band of the resting-state HRP with that for the five model complexes of HRP-I allows the selection of the HRP-I complexes that lead to the observed reduction in intensity. Because oscillator strengths were calculated separately for the B_x and B_y components, the overall oscillator strength for the Soret should be estimated as the sum of these two components. As shown in Fig. 2, *A* and *B*, the oscillator strength of the Soret band is about 2.2 for the resting state of HRP with imh ligand and close to 4.0 for HRP/im^{-1}. For HRP-I, however, it varies for different ground states and different models of the ligand. The calculated oscillator strengths of the Soret band for both the $a_{1u}^{\bullet+}$ (1.5, Fig. 3 *A*) and $a_{2u}^{\bullet+}$ (2.4, Fig. 3 *B*) of HRP-I/imh and $im^{-1}\pi_3^{\bullet+}$ of HRP-I/imh^{-1} (1.9, Fig. 4 *C*) remain comparable with that calculated for the resting-state HRP models (2.2–4.0, Fig. 2, *A* and *B*). In contrast, for both the a_{1u} and a_{2u} radical cations of HRP-I/im^{-1}, (Fig. 4, *A* and *B*) a Soret band with a drastically reduced intensity of $f \leq 0.8$ was found, consistent with the experimental observations. Thus, the HRP-I species appears to be deprotonated and, in this form, both the $a_{1u}^{\bullet+}$ and $a_{2u}^{\bullet+}$ π cation radicals lead to the observed reduction in Soret band intensity.

Analysis of the CI wave functions for the excited states of HRP-I/im^{-1} corresponding to the Soret bands allows the elucidation of the origin of the reduction of the absorption intensity observed in the $a_{1u}^{\bullet+}$ state of HRP-I/im^{-1}. Table 3 lists the frequency and oscillator strengths as well as the 10 excitations with the largest contributions to the B_x and B_y Soret transitions functions of the resting-state HRP and the $a_{1u}^{\bullet+}$ state of the two model HRP-I complexes studied. It can be seen from this table that the Soret band consists of more than the porphyrin $\pi\pi^*$ transitions between the four frontier orbitals, $3a_{2u}$, $1a_{1u}$, $4e_{gx}$, and $4e_{gy}$ originally proposed (Gouterman and Wagniere, 1963). When more orbitals are included in the excitation scheme and the geometry deviates from D_{4h} symmetry, charge transfer (CT) excitations, such as porphyrin to metal and ligand-to-metal transitions, are found to contribute to the Soret band intensity. These transitions occur to a different extent in the resting-state model for HRP and the two HRP-I complexes, and are underlined in Table 3.

It can be seen that increased contribution of charge transfer configurations results in decreased oscillator strengths of the two components (B_x and B_y) of the Soret band. The B_x and B_y states of the resting-state HRP/im^{-1} has the least amount of CT mixing (7–8%) and the calculated oscillator strengths are the largest (1.7–1.9). Similarly, the large oscillator strengths of HRP/imh are also a result of the small CT contribution (16–19%) to the B band. As the CT contribution increases to 28.6 and 34.4% for the B_x component of the Soret of HRP-I/imh and HRP-I/im^{-1}, the oscillator strength decreases to 0.55 and 0.23, respectively. Similarly, decreasing oscillator strength with increasing CT contributions is also observed for the B_y states, from 1.00 of HRP to 0.91 of HRP-I/imh and 0.53 of HRP/im^{-1}. The most important CT transitions that contribute to the Soret band for the HRP-I

TABLE 3 Correlation of the Soret band (B_x and B_y) oscillator strength with the contribution of CT components

HRP/im^{-1}			HRP/im			HRP-I/imh, 1a$_{1u}$$^{\bullet+}$			HRP-I/im^{-1}, 1a$_{1u}$$^{\bullet+}$		
E(B$_x$)	30.5	30.2	E(B$_x$)	29.9	29.6	E(B$_x$)	30.0	30.0	E(B$_x$)	27.7	27.8
f(B$_x$)	1.90	1.69	f(B$_x$)	1.20	1.00	f(B$_x$)	0.55	0.91	f(B$_x$)	0.23	0.53
$3a_{2u}-4e_{gy}$	0.59	$3a_{2u}-4e_{gx}$ 0.62	$3a_{2u}-4e_{gy}$	0.34	$3a_{2u}-4e_{gx}$ 0.27	$3a_{2u}-4e_{gx}$	0.42	$3a_{2u}-4e_{gy}$ 0.54	$3a_{2u}-4e_{gx}$	0.48	$3a_{2u}-4e_{gy}$ 0.48
$1a_{1u}-4e_{gx}$	0.21	$1a_{1u}-4e_{gy}$ 0.20	$2a_{2u}-4e_{gy}$	0.17	$1a_{1u}-4e_{gy}$ 0.12	$3a_{2u}-Fe{=}O\pi_y^*$	0.15	$3a_{2u}-Fe{=}O\pi_y^*$ 0.08	$3a_{2u}-Fe{=}O\pi_y^*$	0.17	$3a_{2u}-Fe{=}O\pi_y^*$ 0.15
$2b_{2u}-4e_{gx}$	0.06	$2b_{2u}-4e_{gy}$ 0.07	$1a_{1u}-4e_{gx}$	0.14	$2a_{2u}-4e_{gx}$ 0.12	$2a_{2u}-4e_{gx}$	0.05	$1a_{1u}-4e_{gx}$ 0.06	$im^{-1}N_\delta sp^2-4e_{gx}$	0.06	$im^{-1}N_\delta sp^2-4e_{gx}$ 0.08
$2b_{2u}-Fe3d_{xz}$	0.06	$2b_{2u}-Fe3d_{xz}$ 0.05	$2a_{2u}-Fe3d_{xz}$	0.09	$3e_{gy}-4e_{gy}$ 0.10	$1a_{1u}-4e_{gy}$	0.05	$2a_{2u}-4e_{gy}$ 0.06	$Fe{=}O\pi_y-1a_{1u}$	0.05	$2b_{2u}-4e_{gx}$ 0.06
$1a_{1u}-2a_{1u}$	0.04	$3e_{gx}-2a_{1u}$ 0.01	$2b_{2u}-4e_{gx}$	0.06	$2a_{2u}-Fe3d_{xz}$ 0.08	$3a_{2u}-2b_{1u}$	0.03	$Fe{=}O\pi_y-Fe3d_{xy}$ 0.04	$2b_{2u}-4e_{gy}$	0.05	$1a_{1u}-4e_{gx}$ 0.05
$3a_{2u}-Fe3d_{yz}$	0.01	$3a_{2u}-Fe3d_{yz}$ 0.01	$3a_{2u}-Fe3d_{xz}$	0.04	$3e_{gx}-4e_{gx}$ 0.07	$Fe{=}O\pi_y-1a_{1u}$	0.03	$3e_{gx}-Fe3d_{xy}$ 0.04	$3e_{gx}-2b_{1u}$	0.03	$3e_{gy}-2b_{1u}$ 0.03
$3e_{gx}-4e_{gy}$	0.01	$im\pi_z-Fe3d_{xy}$ 0.01	$3e_{gy}-4e_{gx}$	0.04	$3e_{gy}-2b_{1u}$ 0.04	$imh\pi_z-1a_{1u}$	0.03	$Fe{=}O\pi_z-1a_{1u}$ 0.03	$2a_{2u}-4e_{gx}$	0.02	$2a_{2u}-4e_{gy}$ 0.02
$im\pi_z-Fe3d_{yz}$	0.01	$3a_{2u}-2a_{1u}$ 0.00	$3e_{gx}-2b_{1u}$	0.02	$3a_{2u}-Fe3d_{xz}$ 0.04	$3e_{gx}-Fe3d_{xy}$	0.03	$2b_{2u}-4e_{gx}$ 0.02	$imh\pi_z-4e_{gx}$	0.02	$2e_{gx}-2b_{1u}$ 0.02
$im\pi_z-4e_{gx}$	0.00	$3a_{2u}-5e_{gx}$ 0.00	$1a_{1u}-3b_{2u}$	0.02	$imh\pi_z-4e_{gx}$ 0.03	$Fe{=}O\pi_y-Fe3d_{xy}$	0.03	$3a_{2u}-imh\pi_z^*$ 0.02	$1a_{1u}-4e_{gy}$	0.01	$Fe{=}O\pi_z-Fe3d_{xy}$ 0.01
$3a_{2u}-3b_{2u}$	0.00	$3e_{gx}-Fe3d_{xz}$ 0.00	$1a_{1u}-imh\pi_z^*$	0.02	$2b_{2u}-Fe3d_{xz}$ 0.02	$2b_{2u}-4e_{gy}$	0.02	$2e_{gx}-1a_{1u}$ 0.02	$im^{-1}N_\delta sp^2-Fe{=}O\pi_z^*$	0.01	$im^{-1}N_\delta sp^2-Fe{=}O\pi_z^*$ 0.01
Total	0.99	Total 0.97	Total	0.94	Total 0.89	Total	0.84	Total 0.91	Total	0.90	Total 0.91
Total CT	0.08	Total CT 0.07	Total CT	0.15	Total CT 0.17	Total CT	0.27	Total CT 0.21	Total CT	0.31	Total CT 0.25
%CT	8.0	%CT 7.2	%CT	16.0	%CT 19.1	%CT	28.6	%CT 23.1	%CT	34.4	%CT 27.5

Only the first 10 configurations with the largest coefficients are included. Charge transfer transitions are underlined.

complexes are porphyrin π to Fe=0 transitions; contributions from the Fe=0 to porphyrin π^* transitions are considerably smaller. For HRP-I/im^{-1}, ligand to porphyrin transitions also become significant for compound I, providing an additional factor for the decreasing of intensity. Thus, the observed reduction of Soret intensity is a result of the mixing of both forward and backward iron-porphyrin charge transfer transitions to the porphyrin $\pi\pi^*$ transitions, as most dramatically demonstrated in the B_x wave function of HRP-I/im^{-1}. The drastic intensity reduction in the Soret band occurs for the HRP-I complex with an im^{-1} ligand and lead to its selection as the preferred model for HRP-I.

For the a_{2u} radical cations of the im^{-1} model, a similar reduction of oscillator strength was calculated and found to have the same origin, mixing of CT transitions. Because the calculated ground-state properties and reduction in intensity of the Soret band are consistent with either an $a_{1u}{}^{\bullet+}$ or $a_{2u}{}^{\bullet+}$ ground state for HRP-I/im^{-1}, the question remains, are there any features of the calculated spectra, other than the reduced intensity, that distinguish these two states, particularly the observed subtle differences in the Q bands region?

For such a detailed comparison between the spectra of the a_{1u} and a_{2u} radical cations of HRP-I/im^{-1}, the complete calculated spectra are listed in Tables 4 and 5. The experimental spectrum of HRP-I is also included in the tables. For both calculated spectra, the excited state that is composed of almost pure porphyrin $\pi\pi^*$ excitations ($1a_{1u}$-$4e_g$ and $3a_{2u}$-$4e_g$) with a moderate oscillator strength is regarded as the origin of the Q band. The most obvious difference between the calculated spectra of the two radical cations is that the excitation energies for the Q band is about 1800 cm^{-1} (5.15 kcal/mol) higher for the a_{1u} radical cation than that in the a_{2u} radical cation. Another feature more useful in distinguishing the two states of HRP-I is the relative energies of the remaining weak absorptions found in the visible region. For HRP-I/im^{-1}, quart-triplet states resulted from the spin coupling between the porphyrin and the Fe atoms were found to have small oscillator strengths near 12 kK ($4^4A''$ and $4^4A'$) and near 15 kK ($6^4A''$ and $6^4A'$), corresponding to the shoulder observed at the lower energy side of the Q band at 15.5 kK. In contrast, for the a_{2u} radical cation weak absorptions ($8^4A'$ and $6^{4\prime\prime}$) were calculated at the higher energy side of the Q band. Comparing these results with experimental spectra, it appears that the calculated visible spectrum of the a_{1u} radical cation of HRP-I/im^{-1} is more consistent than that of the a_{2u} radical cation.

The profile of the observed visible spectrum of CAT-I displays a Q band at 15.1 kK and some shoulder structures at the higher energy side near 16 and 18 kK. The calculated spectra of both a_{1u} and a_{2u} radical cations of CAT-I show weak absorptions above Q, as shown in Tables 6 and 7, although there are more such states for the a_{2u} radical cation ($7^4A'$, $8^4A''$, and $9^4A''$) than for the a_{1u} radical cation ($9^4A''$). Weak absorptions are also calculated at the lower energy side of Q for both radical cations. Thus, the visible spectra of $a_{1u}{}^{\bullet+}$ and $a_{2u}{}^{\bullet+}$ of CAT-I are found to be too similar to be distinguished by comparing with experiment, and both are consistent with the experimental visible spectrum.

TABLE 4 Calculated Spectra for the a_{1u} Radical Cation of HRP-I with an imidazole anion ligand

State	ΔE(kK)	f	Polarity	Main excitations		c^{2}*	Lable‡	Observed
$2^4A'$	8.3	0.000	z	impi3+1a1u	- 1a1u−impi3	0.99	$im^{\bullet+}$	
$2^4A''$	8.7	0.000		dxx−yy	- dxy	1.00	d-d	
$3^4A'$	12.6	0.000		3a2u	- 4egx	0.93	qtx	
$3^4A''$	12.6	0.000		3a2u	- 4egy	0.90	qty	
$4^4A''$	12.7	0.003	y	3egx−pix	- 1a1u−impi3	0.44	$3egx^{\bullet+}$	
				1a1u−impi3	- 4egx	0.34		
$5^4A''$	14.2	0.000		dxx−yy	- pi*y	0.91	d-d2x	
$4^4A'$	12.8	0.002	x	3egy−piy	- 1a1u−impi3	0.43	$3egy^{\bullet+}$	
				1a1u−impi3	- 4egy	0.39		
$5^4A'$	14.6	0.000		dxx−yy	- pi*x	0.88	d-d2y	
				pi*y	- dxy	0.11		
$6^4A''$	15.4	0.005	y	3a2u	- 4egy	0.41	qty	15.5 (sh)
				3egx−pix	- 1a1u−impi3	0.26		
				1a1u−impi3	- 4egx	0.23		
$6^4A'$	15.5	0.003	x	3a2u	- 4egx	0.45	qtx	
				3egy−piy	- 1a1u−impi3	0.31		
				1a1u−impi3	- 4egy	0.17		
$7^4A''$	17.0	0.018	y	3a2u	- 4egy	0.38	Qy	
				2egx+Nsp2	- 1a1u−impi3	0.22		
				1a1u−impi3	- 4egx	0.16		
				2a2u+Nsp2	- 1a1u−impi3	0.11		
$7^4A'$	17.1	0.039	x	3a2u	- 4egx	0.34	Qx	17.4 (w)
				2egy	- 1a1u−impi3	0.33		
				1a1u−impi3	- 4egy	0.18		
$16^4A'$	24.4	0.003	x	3egy−piy	- 4egy	0.33		
				3egx−pix	- 4egx	0.32		
$21^4A''$	25.6	0.092	y	pix	- 1a1u−impi3	0.58	CT1y	
$24^4A''$	26.9	0.056	y	Nsp2−2a2u	- 4egy	0.27	CT2y	
				2b2u	- 4egx	0.21		
$19^4A'$	26.9	0.094	x	Nsp2−2a2u	- 4egx	0.26	CT2x	
				2b2u	- 4egy	0.20		
$20^4A'$	27.4	0.256	x	piy	- 1a1u−impi3	0.24	CT1x	
				2egy	- 1a1u−impi3	0.15		
				Nsp2−2a2u	- 4egx	0.11		
$21^4A'$	27.7	0.232	x	3a2u	- 4egx	0.48	Bx	
				3a2u	- pi*x	0.17		
$27^4A''$	27.8	0.529	y	3a2u	- 4egy	0.48	By	25.1 (s)
				3a2u	- pi*y	0.15		
$29^{4A''}$	28.4	0.002	y	im pi2	- 4egx	0.42		
				pi*y	- 4egx	0.23		
				3egy-piy	- 4egx	0.12		
$22^4A'$	28.4	0.004	xz	im pi2	- 4egy	0.44		
				pi*y	- 4egy	0.34		
$24^4A'$	28.7	0.012	x	im pi2	- 4egy	0.63		
				3egy−piy	- 4egy	0.12		
$32^4A''$	29.4	0.149	y	impi3+1a1u	- 4egx	0.27	CT3y	T28.4(sh)
				2a2u+Nsp2	- 1a1u−impi3	0.10		
$33^4A''$	29.5	0.052	y	3egx−pix	- 4egy	0.35		
$29^4A'$	29.7	0.020	xz	impi3+1a1u	- 4egy	0.80	CT3x	
$34^4A''$	29.9	0.080	y	impi3+1a1u	- 4egx	0.56		

All excited states below 20 kK are listed. For states between 20 and 30 kK, only those with $f > 0.01$ are listed.

*The quantity c^2 is the fractional contribution of each configuration to a given excited state.

‡Charge transfer states are labeled as $im^{\bullet+}$, CT1x, etc; Fe d→d states are labeled as d-d; and the mostly silent quart-triplet states resulted from the spin-coupling between the Fe atom and the poyphine are labeled as qtx, etc.

Additional features that may differentiate the a_{1u} and a_{2u} radical cations of HRP-I and CAT-I in the calculated spectra can also be found. For example, several CT transitions were found below the B band for the $a_{1u}^{\bullet+}$ of HRP-I/im^{-1} and both $a_{1u}^{\bullet+}$ and $a_{2u}^{\bullet+}$ of CAT-I, and no such states were found for the $a_{2u}^{\bullet+}$ of HRP-I/im^{-1}. These are Fe=0 to porphyrin (CT1) and im^{-1} to porphyrin (CT2) transitions. However, because these states have very similar excitation energies as the

TABLE 5 Calculated spectra for the a_{2u} radical cation of HRP-I with an imidazolate anion ligand

State	ΔE (kK)	f	Polarity	Main excitations		c^2	Label	Obeserved
$2^4A'$	7.5	0.000		impi3+1a1u	- 3a2u	0.73	$im^{\bullet+}$	
				1a1u−impi3	- 3a2u	0.25		
$3^4A'$	9.7	0.000		dxx−yy	- dxy	1.00	d-dl	
$4^4A'$	11.8	0.000		1a1u−impi3	- 4egx	0.68	qtx	
				impi3+1a1u	- 4egx	0.27		
$2^4A''$	11.8	0.000		1a1u−impi3	- 4egy	0.70	qty	
				impi3+1a1u	- 4egy	0.25		
$3^4A''$	12.6	0.000	*x*	3egx−pix	- 3a2u	0.43	$3egx^{\bullet+}$	
				2a2u−Nsp2	- 3a2u	0.21		
				3a2u	- 4egx	0.20		
$5^4A'$	12.9	0.000		3egy−piy	- 3a2u	0.58	$3egy^{\bullet+}$	15.5(sh)
				3a2u	- 4egy	0.23		
$6^4A'$	15.0	0.000		dxx−yy	- pi*y	0.91		
$7^4A'$	15.2	0.015	*y*	1a1u−impi3	- 4egx	0.55	Qy	
				impi3+1a1u	- 4egx	0.18		
				3a2u	- 4egy	0.16		
$4^4A''$	15.2	0.060	*x*	1a1u−impi3	- 4egy	0.53	Qx	17.4(w)
				3a2u	- 4egx	0.19		
				impi3+1a1u	- 4egy	0.18		
$8^4A'$	17.4	0.002	*y*	im pi2	- 3a2u	0.44	CT1	
				3egy−piy	- 3a2u	0.19		
				piy	- 3a2u	0.11		
$6^4A''$	17.5	0.009	*x*	3a2u	- 4egx	0.26	qtx	
				2egx+Nsp2	- 3a2u	0.17		
				1a1u−impi3	- 4egy	0.12		
				3egx−pix	- 3a2u	0.12		
				Nsp2+2a2u	- 3a2u	0.10		
$10^4A'$	18.5	0.003	*y*	im pi2	- 3a2u	0.43		
				3a2u	- 4egy	0.17	CT1	
				2egy	- 3a2u	0.16		
$18^4A''$	26.4	0.250	*x*	1a1u−impi3	- 4egy	0.37	Bx	
				pix	- 3a2u	0.35		
				impi3+1a1u	- 4egy	0.10		
$24^4A'$	27.0	0.296	*y*	1a1u−impi3	- 4egx	0.48	By	25.1(s)
				impi3+1a1u	- 4egx	0.19		
$29^4A'$	29.1	0.274	*y*	piy	- 3a2u	0.32	CT2y	28.4(sh)
				2egy	- 3a2u	0.23		
$24^4A''$	29.5	0.036	*x*	impi3+1a1u	- dxy	0.61	CT3x	
				1a1u−impi3	- dxy	0.13		
				3egy−piy	- dxy	0.10		
$25^4A''$	29.6	0.072	*x*	impi3−1a1u	- dxy	0.52	CT3x	
				1a1u−impi3	- dxy	0.12		
				3egy−piy	- dxy	0.10		
$33^4A'$	30.3	0.221	*y*	impi3+1a1u	- 4egx	0.36	CT4y	
				1a1u−impi3	- 4egx	0.13		
$31^4A''$	30.3	0.356	*x*	im pix2	- 4egy	0.20	CT4x	
				Nsp2+2a2u	- 3a2u	0.12		
				3egy−piy	- 4egy	0.10		

See footnotes of Table 4.

strong Soret band, they are most likely to be buried and are not useful for comparison with experiment.

It thus appears that the calculated spectra of the a_{1u} radical cations of both HRP-I and CAT-I are consistent with the experimental spectra and can provide a partial explanation for the subtle differences observed between them. However, given the small differences calculated between $a_{1u}^{\bullet+}$ and $a_{2u}^{\bullet+}$ of CAT-I, the visible spectra of these two radical cation alone are not reliable indicators of their ground state symmetry. The calculated energy preference for the $a_{1u}^{\bullet+}$ provides stronger evidence for an $a_{1u}^{\bullet+}$ ground state for both enzymes. Because both enzymes are found to have the same ground-state symmetry, the different functions of these two enzymes may be caused by other factors such as differences in the protein environment.

CONCLUSIONS

The $a_{1u}^{\bullet+}$ of HRP-I/im^{-1} and CAT-I model complexes have been selected as consistent representations of the ground

TABLE 6 Calculated spectra for the a_{1u} radical cation of Cat-I

State	ΔE(kK)	f	polarity	Main excitations		c^2	Label	Observed
$2^4A''$	8.1	0.000		3dxy	- dxx−yy	1.00	d-d1	
$3^4A''$	12.1	0.001	*y*	3egx−pix	- 1a1u	0.56	$3egx^{\bullet+}$	
				1a1u	- 4egx	0.19		
				ph pi3	- 1a1u	0.11		
$4^4A''$	12.4	0.000		3a2u	- 4egy	0.91	qt	
$2^4A''$	12.5	0.000		3a2u	- 4egx	0.90	qt	
$3^4A'$	12.8	0.003	*x*	3egy−piy	- 1a1u	0.42	$3egy^{\bullet+}$	
				1a1u	- 4egy	0.34		
$4^4A'$	13.6	0.000		3dxy	- pi*y	0.87	d-d2y	
				pi*x	- dxx−yy	0.12		
$5^4A''$	14.0	0.003	*y*	ph pi3	- 1a1u	0.64	$ph^{\bullet+}$	
				1a1u	- 4egx	0.18		
$6^4A''$	14.7	0.000		3dxy	- pi*x	0.79	d-d2x	
				pi*y	- dxx−yy	0.20		
$5^4A'$	15.2	0.002	*x*	3a2u	- 4egx	0.46	qt	
				1a1u	- 4egy	0.21		
				3egy−piy	- 1a1u	0.18		
$7^4A''$	15.3	0.003	*y*	3a2u	- 4egy	0.46	qt	
				3egx−pix	- 1a1u	0.21		
				1a1u	- 4egx	0.16		
$6^4A'$	17.0	0.051	*x*	3a2u	- 4egx	0.34	Qx	15.1(m)
				2egy	- 1a1u	0.28		
				1a1u	- 4egy	0.22		
$8^4A''$	17.1	0.029	*y*	3a2u	- 4egy	0.30	Qy	
				2egx	- 1a1u	0.26		
				1a1u	- 4egx	0.21		
$9^4A''$	17.2	0.002	*y*	2b2u	- 1a1u	0.54	qt	16.7, 18.8(sh)
				3egx−pix	- 4egy	0.12		
$11^4A'$	23.9	0.013	*xz*	ph pi3	- 4egx	0.41	CT1x	
				3egy−piy	- 4egy	0.15		
$12^4A'$	24.3	0.017	*x*	ph pi3	- 4egx	0.68	CT1x	
$19^4A''$	24.3	0.048	*y*	ph pi3	- 4egy	0.68	CT1y	
$20^4A''$	24.5	0.016	*y*	ph pi3	- 4egy	0.47	CT1y	
				3egx−pix	- 4egy	0.20		
$13^4A'$	24.9	0.022	*x*	3egx−pix	- 4egx	0.47	CT2x	
				ph pi3	- 4egx	0.13		
$22^4A''$	26.0	0.037	*y*	01px+02px	- 1a1u	0.48	CT3y	
				sigma−pix	- 1a1u	0.14		
$19^4A'$	27.5	0.025	*x*	2b2u	- 4egx	0.31	Bx(sh)	
				2a2u	- 4egx	0.17		
				ph pi3	- 4egx	0.10		
				3egy−piy	- 2b1u	0.10		
$22^4A'$	28.0	0.182	*x*	3a2u	- 4egx	0.28	Bx	
				3a2u	- pi*x	0.26		
$26^4A''$	28.1	0.432	*y*	3a2u	- 4egy	0.39	By	24.9(s)
				3a2u	- pi*y	0.15		
				ph pi3	- 4egy	0.13		
$27^4A''$	28.6	0.012	*y*	02py+01py	- 4egx	0.37	CT4y	
				3egy−piy	- 4egx	0.19		
$28^4A''$	28.7	0.050	*y*	3egx−pix	- 4egy	0.26	CT5y	
				3a2u	- 2b1u	0.18		
$29^4A''$	28.7	0.029	*y*	3a2u	- 2b1u	0.37	CT6y	
				2egx	- 4egy	0.13		
				3egx−pix	- 4egy	0.11		
				2egy	- 4egx	0.10		
$25^4A'$	28.9	0.090	*x*	02py+01py	- 4egy	0.27	CT4x	
				2egy	- 1a1u	0.12		
$26^4A'$	29.0	0.166	*x*	02py+01py	- 4egy	0.23	CT4x	
				2egy	- 1a1u	0.10		
$29^4A'$	29.8	0.287	*x*	3a2u	- pi*x	0.35	CT7x	28.6(sh)
				3a2u	- 4egx	0.27		

See footnotes of Table 4.

TABLE 7 Calculated spectra for the a_{2u} radical cation of Cat-I

State	ΔE(kK)	f	polarity	Main excitations		c^2	Label	Observed
$2^4A'$	9.0	0.000		dxy	- dxx−yy	1.00	d-d1	
$2^4A''$	11.4	0.005	*xz*	3egx−pix	- 3a2u	0.38	$3egx^{\bullet+}$	
				ph pi3	- 3a2u	0.31		
				1a1u	- 4egy	0.16		
$3^4A''$	11.4	0.001	*xz*	1a1u	- 4egy	0.81	q,t	
$3^4A'$	11.5	0.000		1a1u	- 4egx	0.96	q,t	
$4^4A'$	12.7	0.000		3egy−piy	- 3a2u	0.63	$3egy^{\bullet+}$	
				3a2u	- 4egy	0.17		
$4^4A''$	13.2	0.008	*z*	ph pi3	- 3a2u	0.53	$ph^{\bullet+}$	
				3egx−pix	- 3a2u	0.25		
				3a2u	- 4egx	0.12		
$5^4A''$	14.0	0.000		dxy	- pi*y	0.87	d-d2y	
				pi*x	- dxx−yy	0.12		
$6^4A''$	14.8	0.056	*x*	1a1u	- 4egy	0.75	Qx	15.1(m)
				3a2u	- 4egx	0.18		
$5^4A'$	14.8	0.016	*y*	1a1u	- 4egx	0.74	Qy	
				3a2u	- 4egy	0.19		
$6^4A'$	15.4	0.000		dxy	- pi*x	0.77	d-d2x	
				pi*y	- dxx−yy	0.22		
$7^4A'$	16.9	0.005	*y*	02py+01py	- 3a2u	0.51		16.7(sh)
				3a2u	- 4egy	0.19		
				2egy	- 3a2u	0.11		
				1a1u	- 4egx	0.10		
$8^4A''$	17.9	0.008	*xz*	pi*x	- dxx−yy	0.40	d-d	
				3a2u	- 4egx	0.19		
				2egx	- 3a2u	0.11		
$9^4A''$	18.1	0.007	*xz*	pi*x	- dxx−yy	0.42	d-d	18.8(sh)
				3a2u	- 4egx	0.15		
				2egx	- 3a2u	0.11		
$16^4A''$	25.8	0.242	*x*	01px+02px	- 3a2u	0.29	CT1x	
				1a1u	- 4egy	0.27		
				ph pi3	- 4egx	0.13		
$20^4A'$	25.9	0.188	*y*	ph pi3	- 4egy	0.52	CT2y	
				1a1u	- 4egx	0.22		
$23^4A'$	27.3	0.199	*y*	1a1u	- 4egx	0.49	By	24.9(s)
				ph pi3	- 4egy	0.18		
				2egy	- 3a2u	0.11		
$19^4A''$	27.4	0.119	*x*	1a1u	- 4egy	0.43	Bx	
				2egx	- 3a2u	0.17		
				ph pi3	- 4egx	0.10		
$29^4A'$	29.6	0.014	*y*	3egy−piy	- 4egx	0.39	CT3y	
				pi*y	- 4egx	0.14		
				02py+01py	- 4egx	0.11		
$31^4A'$	30.4	0.352	*y*	ph pi3	- 4egy	0.25	CT4y	28.6(sh)
				2egy	- 3a2u	0.16		

See footnotes in Table 4.

states of these reactive intermediates of the two enzymes based on the comparison of a number of calculated properties with experiment. For both HRP-I and CAT-I, the a_{1u} radical cation was calculated to be the lowest in energy and was further stabilized by the inclusion of porphyrin substituents. All of the low-lying states of the active site models of HRP-I, including the $a_{1u}^{\bullet+}$ of HRP-I/im^{-1}, have been found to have a similar spin distributions on the Fe=O moiety. Thus, differences in spin distributions cannot be used to select the most plausible model. Calculated nuclear quadrupole splittings and Soret bands with significantly decreased intensities relative to the resting state also indicate that either $a_{1u}^{\bullet+}$ or $a_{2u}^{\bullet+}$ of HRP-I/im^{-1} can be responsible for their experimental spectra. Other features of the calculated visible spectrum of the $a_{1u}^{\bullet+}$ of HRP-I/im^{-1} are more consistent with the experimental spectrum of HRP-I. For CAT-I, the calculated spectra of both a_{1u} and a_{2u} radical cations of CAT-I are similar. Thus, although less definitive for CAT-I, all of the properties calculated are consistent with an $a_{1u}^{\bullet+}$ ground state of both HRP-I and CAT-I with the axial ligand of HRP-I being a deprotonated histidine, and the energy of the $a_{1u}^{\bullet+}$ is lower than the $a_{2u}^{\bullet+}$ state. Thus, it appears that the distinct function of CAT and HRP cannot be attributed to different ground states of their Compound I. Other factors, such as different

protein environments in the catalytic centers, may play a more direct role in determining function.

The Support of National Science Foundation Grant DMB-9096181 is gratefully acknowledged.

REFERENCES

Andersson, L. A., and J. H. Dawson. 1991. EXAFS spectroscopy of heme-containing oxygenases and peroxidases. *In* Metal Complexes with Tetrapyrrole Ligands, Vol 2, J. W. Buchler, editor Springer-Verlag, Berlin, 1–40.

Bacon, A. D. and M. C. Zerner. 1979. An intermediate neglect of differential overlap theory for transition metal complexes: Fe, Co and Cu chlorides. *Theor. Chim. Acta.* 53:21–54.

Bosshard, H. R., H. Anni, and T. Yonetani. 1991. Yeast cytochrome *C* peroxidase. *In* Peroxidases in Chemistry and Biology, Vol 2. J. Everse, K. Everse, and M. B. Grisham, editors. CRC Press, Boca Raton, FL. 51–84.

Browett, W. R., and M. J. Stillman. 1981. Evidence for heme π cation radical species in compound I of horseradish peroxidase and catalase. *Biochim. Biophys. Acta.* 660:1–7.

Chance, B., L. Powers, Y. Ching, T. Poulos, G. R. Schonbaum, I. Yamazaki, and K. G. Paul. 1984. X-ray absorption studies of intermediates in peroxidase activity. *Arch. Biochem. Biophys.* 235:596–611.

Chuang, W.-J., and H. E. Van Wart. 1992. Resonance Raman spectra of horseradish peroxidase and bovine liver catalase compound I species. Evidence for predominant 2A2u pi-cation radical ground state configurations. *J. Biol. Chem.* 267:13293–13301.

de Ropp, J. S., V. Thanabal, and G. N. La Mar. 1985. NMR evidence for a horseradish peroxidase state with a deprotonated proximal histidine. *J. Am. Chem. Soc.* 107:8268–8720.

Dolphin, D., A. Forman, D. C. Borg, J. Fajer, and R. H. Felton. 1971. Compounds I of catalase and horse radish peroxidase: π cation radicals. *Proc. Natl. Acad. Sci. USA.* 68:614–618.

Dolphin, D. 1981. The electronic configuration of catalases and peroxidases in their high oxidation states: a difinitive assessment. *Isr. J. Chem.* 21: 67–71.

Du, P., F. U. Axe, G. H. Loew, S. Canuto, and M. C. Zerner. 1991. Theoretical study on the electronic spectra of model compound II complexes of peroxidases. *J. Am. Chem. Soc.* 113:8614–8621.

Dunford, H. B., 1982. Peroxidases. *Adv. Inorg. Biochem.* 4:41–68.

Dunford, H. B., 1991. Horseradish peroxidase: structure and kinetic properties. *In* Peroxidases in Chemistry and Biology, Vol. 2. J. Everse, K. Everse, and M. B. Grisham, editors. CRC Press, Boca Raton, FL 1–24.

Edwards, W. D., and M. C. Zerner. 1987. A generalized restricted open-shell Fock operator. *Theor. Chim. Acta.* 72:347–361.

Edwards, W. D., B. Weiner, and M. C. Zerner. 1986. On the low-lying states and electronic spectroscopy of iron (II) porphine. *J. Am. Chem. Soc.* 108:2196–2204.

Edwards, W. D., B. Weiner, and M. C. Zerner. 1988. The electronic structure and spectra of various spin states of porphinato iron (III) chloride. *J. Phys. Chem.* 92:6188–6197.

Fita, I., and M. G. Rossmann. 1985. The active center of catalase. *Proc. Natl. Acad. Sci. USA.* 82:1604–1608.

Gouterman, M., and G. H. Wagniere. 1963. Spectra of porphyrins, part II. Four orbital model. *J. Mol. Spectrosc.* 11:108–127.

Hager, L. P., D. L. Doubek, R. M. Silverstein, J. H. Hager, and J. C. Martin. 1972. Chloroperoxidase. IX. The structure of compound I. *J. Am. Chem. Soc.* 94:4364–4366.

Hanson, L. V., C. K. Chang, M. S. Davis, and J. Fajer. 1981. Electron pathways in catalase and peroxidase enzymic catalysis. Metal and macrocycle oxidations of iron porphyrins and chlorins. *J. Am. Chem. Soc.* 103:663–670.

Harrison, J. R., T. Araiso, M. M. Palcic, and H. B. Dunford. 1980. Compound I of myeloperoxidase. *Biochem. Biophys. Res. Commun.* 94:34–40.

Hewson, W. D., and L. P. Hager. 1978. Peroxidases, catalases, and chloroperoxidase. *In* Porphyrins, Vol. 7. D. Dolphin, editor. Academic Press, New York. 295–331.

La Mar, G. N., V. Thanabal, R. D. Johnson, K. M. Smith, and D. W. Parish. 1989. Deuterium NMR study of structural and dynamic properties of horseradish peroxidase. *J. Biol. Chem.* 264:5428–5434.

Loew, G. H., Z. S. Herman. 1980. Calculated spin densities and quadrupole splitting for model horseradish peroxidase compound I: evidence for iron (IV) porphyrin (S-1) π cation radical electronic structure. *J. Am. Chem. Soc.* 102:6173–6174.

Moss, T. H., A. Ehrenberg, and A. J. Bearden. 1969. Mossbauer spectroscopic evidence for the electronic configuration of iron in horseradish peroxidase and its peroxide derivatives. *Biochemistry.* 8:4159–4162.

Paeng, K.-J., and J. R. Kincaid. 1988. The resonance Raman spectrum of horseradish peroxidase compound I. *J. Am. Chem. Soc.* 110:7913–7915.

Palcic, M. M., and H. B. Dunford. 1980. The reaction of human erythrocyte catalase with hydroperoxides to form compound I. *J. Biol. Chem.* 255: 6128–6132.

Palcic, M. M., R. Rutter, T. Araiso, L. P. Hager, and H. B. Dunford. 1980. Spectrum of chloroperoxidase compound I. *Biochem. Biophys. Res. Commun.* 94:1123–1127.

Pauncz, R. 1979. Spin Eigenfunctions: Construction and Use. Plenum Press, New York.

Penner-Hahn, I. E., K. S. Eble, T. J. McMurry, M. Renner, A. L. Belch, J. T. Groves, J. H. Dawson, and K. O. Hodgson. 1986. Structural characterization of horseradish peroxidase using EXAFS spectroscopy. Evidence for Fe=O ligation in compounds I and II. *J. Am. Chem. Soc.* 108:7819–7825.

Piciulo, P. L., G. Rupprecht, and W. R. Scheidt. 1974. Stereochemistry of nitrosylmetalloporphyrins. Nitrosyl-$\alpha,\beta,\gamma,\delta$ tetraphenylporphinato (4-methylpiperidine)manganese. *J. Am. Chem. Soc.* 96:5293–5295.

Poulos, T. L., and B. C. Finzel. 1984. Heme enzyme structure and function. *In* Peptide and Protein Reviews, Vol. 4. M. T. W. Hearn, editor. Marcel Dekker, New York. 115–162.

Ridley, J., and M. Zerner. 1973. An intermediate neglect of differential overlap technique for spectroscopy: pyrrole and the azines. *Theor. Chim. Acta.* 32:111–134.

Ridley, J. E., and M. C. Zerner. 1976. Triplet states via intermediate neglect of differential overlap: benzene, pyridine and the diazines. *Theor. Chim. Acta.* 42:223–236.

Roberts, J. E., B. M. Hoffman, R. Rutter, and L. P. Hager. 1981. Electron-nuclear double resonance of horseradish peroxidase compound I. *J. Biol. Chem.* 256:2118–2121.

Schulz, C. E., P. W. Devaney, H. Winkler, P. G. Debrunner, N. Doan, R. Chiang, R. Rutter, and L. P. Hager. 1979. Horseradish peroxidase compound I: evidence for spin coupling between the heme iron and a "free" radical. *FEBS Lett.* 103:102–105.

Schulz, C. E., R. Rutter, J. T. Sage, P. G. Debrunner, and L. P. Hager. 1984. Mossbauer and electron paramagnetic resonance studies of horseradish peroxidase and its catalytic intermediates. *Biochemistry.* 23:4743–4754.